Interaction between two inhomogeneously charged parallel surfaces in the strong coupling regime

Y. S. Jho,[1,*] G. Park,[1] C. S. Chang,[1,2] P. Pincus,[1,3] and M. W. Kim[1,3]
[1]*Department of Physics, Korea Advanced Institute of Science and Technology, Yuseong-Gu, Daejeon, Korea 305-701*
[2]*Courant Institute of Mathematical Sciences, New York University, 251 Mercer Street, New York, New York 10012, USA*
[3]*Materials Research Laboratory, University of California at Santa Barbara, Santa Barbara, California 93106, USA*
(Received 19 July 2005; revised manuscript received 14 November 2005; published 6 February 2006)

The counterion density profile and pressure between two inhomogenously charged parallel plates are analyzed analytically and numerically in the strong-coupling regime. Point charges are used and the surface charges are immobile. It is found that when the surface charge distribution is inhomogeneous, the charge coupling effect becomes stronger, the counterion spatial distribution is more localized toward the plate surfaces, and, thus, the pressure between two plates becomes lower than in the case when the surface charge distribution is homogeneous.

DOI: 10.1103/PhysRevE.73.021502 PACS number(s): 61.20.Ja, 82.45.−h, 82.70.−y, 61.20.Qg

I. INTRODUCTION

One of the fundamental forces that governs biological systems is the Coulomb interaction. Many phenomena in biological systems (for example, interacting polyelectrolytes, transport across membranes, or polymer adsorption and desorption kinetics at membranes) are based on the Coulomb interaction. These biological systems are composed of charged macroanions and counterions. For planar macroanions, the system is often modeled with uniformly charged anion plates and pointlike counterions [1–8]. This simplified system has been studied both analytically and numerically by many authors using a popular theoretical tool: the mean field theory in the Poisson-Boltzmann approximation. This theoretical tool, however, corresponds to the lowest order perturbation theory and is valid in the weak-coupling limit to represent the case when the thermal energy is higher than the Coulomb potential energy.

In a real biological system, the system is usually strongly coupled. The interaction potential energy is much higher than the thermal energy. Guldbrand *et al.* [9] and Ha [10] found from computer simulations that two identical highly (and uniformly) charged plates may be able to attract each other by counterion bridging. This does not agree with the result from the mean field theory, which always gives a repulsive pressure between two identically charged surfaces. Recently, a strong-coupling analytic theory [11] has been developed, which shows excellent agreement with Monte Carlo simulation results [1] in a one-plate system.

Moreover, molecular structure requires that the charge distribution on most biological surfaces is intrinsically discrete. Netz *et al.* [12,13] applied the strong-coupling theory to the case where a single plate is discretely charged and found that the counterions exhibit a strongly concentrated, laterally averaged density at the surface. Even in the weak-coupling regime, a similar trend has been observed by Lukatsky *et al.* [14]. Using the Poisson-Boltzmann theory combined with a Monte Carlo simulation in the weak-coupling regime, Ref. [14] showed that the pressure between identical anionic surfaces is reduced by the surface charge modulation, accompanied by the depletion of the counterion density near the midplane. In addition, Henle *et al.* [15] developed a two-state analytic model for a one-plate system to interpolate in the region between the strong-coupling and weak-coupling regimes. They also found that the discretization of the surface anionic charge distribution can enhance localization of the counterion density to the surface.

Even though many strongly coupled biological interactions may be approximately modeled by two inhomogeneously charged plates with counterions in between, there have not been any such numerical simulations reported in the literature to our knowledge. Strongly coupled parallel plate systems have been studied with homogeneous surface charge only [9,10]. The previous studies of inhomogeneously charged plate systems have been either weak coupling with two plates [14] or strong coupling with one plate [13].

In the present work, a systematic study on the effects of discretization or modulation of the surface charge on the counterion spatial distribution and the pressure response between two charged plates is performed in the strong-coupling limit. As the first step for understanding the complicated inhomogeneous and strongly coupled system, we use point charges in the present work, with the understanding that the results may be modified by the finite size effect to be developed in the future. Both analytical and numerical methods are used. The dependence of the physical properties on several key physical parameters is examined and identified.

The paper is organized as follows. In Sec. II, an analytical theory is used to obtain explicit strong-coupling forms for the spatial density profile and pressure response between two charged surfaces with periodic surface charge distributions. Various competing physical mechanisms are discussed. In Sec. III, results obtained from the numerical molecular dynamics simulations are presented and compared to the analytical results obtained in Sec. II. Section IV contains a summary and concluding remarks.

*Electronic address: joys@kaist.ac.kr

II. ANALYTIC DESCRIPTION OF A STRONGLY COUPLED PARTICLE SYSTEM BETWEEN TWO CHARGE-MODULATED SURFACES

Two inhomogeneously charged planar plates with point-like counterions are assumed in the present analytic study. The counterions (cations) are assumed to be confined between the two parallel surfaces, neutralizing the total net charge in the system. The regular surface charge density distributions on each of the plates may have phase differences from one another, $-e\sigma_1(x,y)$ and $-e\sigma_2(x,y)$, but both have the same average charge density number $\sigma_0=q_0N/2L^2$, where N is the total number of counterions within the surface area L^2 and q_0 denotes the charge valence of the counterions. Assuming a square lattice per surface macroion with lattice constant a, the surface charge densities may be expressed by the Fourier decomposition

$$\sigma_1(x,y)/\sigma_0 = 1 + 2\epsilon\sum_{p>0}\cos\left(\frac{2\pi}{a}px\right) + 2\epsilon\sum_{q>0}\cos\left(\frac{2\pi}{a}qy\right) + 4\epsilon\sum_{p,q>0}\cos\left(\frac{2\pi}{a}px\right)\cos\left(\frac{2\pi}{a}qy\right),$$

$$\sigma_2(x,y)/\sigma_0 = 1 + 2\epsilon\sum_{p>0}s_p\cos\left(\frac{2\pi}{a}px\right) + 2\epsilon\sum_{q>0}s_q\cos\left(\frac{2\pi}{a}qy\right) + 4\epsilon\sum_{p,q>0}s_{p+q}\cos\left(\frac{2\pi}{a}px\right)\cos\left(\frac{2\pi}{a}qy\right),$$

where (p,q) are positive integers, ϵ is the amplitude of the nonzero (p,q) harmonic mode of the surface charge modulation, and $s_p=(-1)^p$ represents the phase shift of the density modulations between two surfaces. Negative Fourier numbers have been combined into positive numbers. $s_p=1$ if in phase and -1 if out of phase. The surfaces are located at $z=0$ and d. We assume that the charges are located at a depth D from the plate surface. Thus, the distance for the closest approach between counterions and surface charges is assumed to be D (we may consider that the counterion and anion sizes are reflected in D to some extent).

In the formal theoretical formulation, all lengths are normalized to the Guoy-Chapman length $\mu\equiv 1/(2\pi q_0 l_B\sigma_0)$, where $l_B=e^2/4\pi\epsilon_0\epsilon_d k_BT$ is the Bjerrum length and ϵ_d is the solvent dielectric constant. The tilde above a physical quantity represents this normalization. The Coulomb interaction strength compared to the thermal energy is defined as the coupling parameter $\Xi\equiv q_0^2 l_B/\mu=2\pi q_0^3 l_B^2\sigma_0$, which is independent of the plate distance d. In the limit of $\Xi\to 0$ (low surface charge density or high temperature), the Poisson-Boltzmann theory is asymptotically correct. In the opposite limit $\Xi\gg 1$, a strong-coupling physics dominates. A more physically convenient length normalization, the x-y projection of the intercounterion distance $a_\perp$ from $\pi a_\perp^2\sigma_0=q_0$, is used for numerical plots and numerical simulations, as will be shown later in this section. $a_\perp$ is related to μ by $a_\perp/\mu=\sqrt{2\Xi}$.

The Hamiltonian of the system considered is given by

$$\frac{\mathcal{H}}{k_BT} = \Xi\sum_{i>j}\frac{1}{|\tilde{r}_i-\tilde{r}_j|} + \sum_i \tilde{u}(r_i),$$

where the first term is from pair interactions between the counterions at positions $\tilde{r}_i$ and $\tilde{r}_j$, and the second term is the external potential energy due to the fixed surface charges.

The potential energy at $\tilde{r}_i$ from the periodic charges is calculated using a convergence factor as in Ref. [16],

$$\tilde{u}(r_i) = \sum_{k,l\in\mathcal{Z}} 2\pi\frac{1}{\tilde{r}} = \lim_{\beta\to 0}\sum_{k,l\in\mathcal{Z}} 2\pi\frac{e^{-\beta|\tilde{r}_{ij}+n_{kl}|}}{|\tilde{r}_{ij}+n_{kl}|} = \lim_{\beta\to 0}\frac{2\pi}{\tilde{a}^2}\sum_{k,l\in\mathcal{Z}}\frac{e^{-\beta_{kl}|\tilde{z}|}}{\beta_{kl}}e^{2\pi ikx/a}e^{2\pi ily/a}$$

where $\mathcal{Z}$ is a set of integer numbers, β is a real number, $\beta_{kl}=\sqrt{\beta^2+(2\pi k/\tilde{a})^2+(2\pi l/\tilde{a})^2}$, $\tilde{r}_{ij}=(\tilde{x}_i-\tilde{x}_j,\tilde{y}_i-\tilde{y}_j,\tilde{z}_i-\tilde{z}_j)$, and $n_{kl}=(k\tilde{a},l\tilde{a},0)$. After taking $\beta\to 0$, the potential becomes

$$\begin{aligned}\tilde{u}(\tilde{r}) = &-\frac{4\epsilon}{Q_0}\sum_{p,q,>0}\frac{e^{-Q_0 f_{pq}(\tilde{z}+\tilde{D})}}{f_{pq}}\cos(Q_0p\tilde{x})\cos(Q_0q\tilde{y})\\ &-\frac{2\epsilon}{Q_0}\left(\sum_{p>0}\frac{e^{-Q_0 f_p(\tilde{z}+\tilde{D})}}{f_p}\cos(Q_0p\tilde{x}) + \sum_{q>0}\frac{e^{-Q_0 f_q(\tilde{z}+\tilde{D})}}{f_q}\cos(Q_0q\tilde{y})\right)\\ &-\frac{4\epsilon}{Q_0}\sum_{p,q,>0}\frac{e^{-Q_0 f_{pq}(\tilde{d}-\tilde{z}+\tilde{D})}}{f_{pq}}s_{p+q}\cos(Q_0p\tilde{x})\cos(Q_0q\tilde{y})\\ &-\frac{2\epsilon}{Q_0}\left(\sum_{p>0}\frac{e^{-Q_0 f_p(\tilde{d}-\tilde{z}+\tilde{D})}}{f_p}s_p\cos(Q_0p\tilde{x}) + \sum_{q>0}\frac{e^{-Q_0 f_q(\tilde{d}-\tilde{z}+\tilde{D})}}{f_q}s_q\cos(Q_0q\tilde{y})\right),\end{aligned} \tag{1}$$

where $f_p=p$, $f_q=q$, $f_{pq}=\sqrt{p^2+q^2}$, $\omega_p=2\pi f_p$, $\omega_q=2\pi f_q$, $\omega_q=2\pi f_{pq}$, and $Q_0=2\pi\mu/a$.

We first study the simplest case where the charge modulation has only the fundamental Fourier modes $[(p,q)=(1,0)$ and $(0,1)]$. Even if the charge modulation has higher Fourier components, if the normalized depth $\tilde{D}$ of the surface charge is large, the modulated charge effect decays fast with the Fourier mode numbers (p,q) and the essential physics can be captured with only the lowest Fourier modes $[(p,q)=(1,0)$ and $(0,1)]$. The corresponding interaction energy for the simplest charge modulation case is given by

$$\tilde{u}_{in}(\tilde{r}) = -\Gamma_+[\cos(Q_0\tilde{x})+\cos(Q_0\tilde{y})],$$

$$\tilde{u}_{out}(\tilde{r}) = -\Gamma_-[\cos(Q_0\tilde{x})+\cos(Q_0\tilde{y})],$$

$$\Gamma_+ = \frac{4\epsilon}{Q_0} e^{-Q_0(\tilde{d}/2+\tilde{D})} \cosh\left[Q_0\left(\frac{\tilde{d}}{2} - \tilde{z}\right)\right] \tag{2}$$

$$\Gamma_- = \frac{4\epsilon}{Q_0} e^{-Q_0(\tilde{d}/2+\tilde{D})} \sinh\left[Q_0\left(\frac{\tilde{d}}{2} - \tilde{z}\right)\right], \tag{3}$$

where $Q_0 = 2\pi\mu/a$, again, and the subscripts *in* and *out* signify the in-phase and out-of-phase surface charge modulations, respectively, between two plates.

We then briefly review a known analytic strong-coupling method [1,5] before using it to obtain the explicit analytic forms of the counterion density profile and pressure from the above interaction energy $\tilde{u}$. Expanding the partition function in inverse powers of the coupling strength Ξ, corresponding to the conventional virial expansion, we obtain [1]

$$\begin{aligned}\mathcal{Z}_\lambda = \exp\Bigg(& -(1/4\pi^2\Xi)\int d\tilde{r}\, d\tilde{r}'\, \tilde{\sigma}(\tilde{r}) \\ & \times [v(\tilde{r}-\tilde{r}')/2 - v(\tilde{r}-\tilde{r}_0)]\tilde{\sigma}(\tilde{r}')\Bigg) \\ & \times \sum_{j=0}^{\infty} \frac{1}{j!}\left(\frac{\Lambda}{2\pi\Xi}\right)^j \prod_{k=1}^{j}\left[\int d\tilde{r}_k \tilde{\Omega}(\tilde{r}_k)\right] \\ & \times \exp\Bigg(\sum_i w(\tilde{r}_i) - \Xi\sum_{i<j} v(\tilde{r}_i - \tilde{r}_j) - \sum_i \tilde{u}(\tilde{r}_i)\Bigg),\end{aligned}$$

where $v(\tilde{r}_i - \tilde{r}_j) \equiv 1/|\tilde{r}_i - \tilde{r}_j|$, and $\tilde{\Omega}(\tilde{r}_k)$ is unity if $\tilde{r}_k$ is within the integration volume and zero otherwise. The expectation value of the counterion density is a functional derivative of the partition function with respect to the generating field w. The normalized counterion density distribution is then given by [1]

$$\tilde{n}(\tilde{r}) = \frac{n(\tilde{r})}{2\pi l_B \sigma_0^2} = \Lambda e^{-\tilde{u}(\tilde{r})} + O(\Xi^{-1}), \tag{4}$$

where the factor Λ is determined by the normalization condition $\int d\tilde{r}\, \tilde{n}(\tilde{r})/\tilde{L}^2 = 1$. Details of these procedures are described in Refs. [1,5]. In a previous study of a system with a uniformly charged surface [1], this strong-coupling approach represented by Eq. (4) was shown to work well for coupling strength $\Xi \gtrsim 10^4$. It will be shown in the next section that this number will become much lower (as low as 20 has been verified) for nonuniformly charged surfaces, since a nonuniform surface charge distribution tends to strengthen the effective coupling significantly.

We now go back to the fundamental Fourier mode case. The laterally averaged (in x and y) counterion distribution is given by

$$\tilde{n}_\pm(\tilde{z}) = \frac{2I_0^2[\Gamma_\pm(\tilde{z})]}{\int_0^{\tilde{d}} d\tilde{z}\, I_0^2[\Gamma_\pm(\tilde{z})]} \tag{5}$$

where a + sign denotes in phase, a − sign denotes out of phase, I_0 denotes the modified Bessel function of zeroth order, and $\Gamma_\pm$ are defined in Eqs. (2) and (3). Equation (5), with Eqs. (2) and (3), shows that when the surface charge is uniformly distributed (i.e., $\epsilon = 0$; hence, $I_0 = 1$), the corresponding density profile $\tilde{n}_\pm = 2/\tilde{d}$ is constant in $\tilde{z}$. The equations also show that the charge modulation effect is to enhance the counterion density near the plate surfaces for I_0^2, a monotonically increasing function. The counterion density under modulated surface charge has maximum value at the plate surfaces and a minimum value at the center between two plates. The degree of counterion surface localization will be expressed by the density ratio $\tilde{\rho}_{rel} \equiv \tilde{n}(0)/\tilde{n}(\tilde{d}/2)$. It can be seen from Eqs. (2), (3), and (5), that there are several parameters that affect the counterion density profile: the distance between surfaces d, mode amplitude ϵ, Guoy-Chapman length μ, counterion valence q_0, depth of the surface charge D, and the charge distribution phase between two surfaces. It is clear from the above equations that increasing D weakens the density ratio.

Divalent counterions in thermal contact with a thermal reservoir at a normalized temperature (300 K) are used throughout the present work unless otherwise specified. The charge depth D is normalized to the two-dimensional inter counterion distance $a_\perp$, defined by $\pi a_\perp^2 \sigma_0 = q_0$, instead of the Guoy-Chapman length. This is because the coupling strength $\Xi \equiv q_0^2 l_B/\mu = 2\pi q_0^3 l_B^2 \sigma_0 = 2(q_0^2 e^2/4\pi\epsilon_0 a_\perp \epsilon_d k_B T)^2$ is a simpler explicit function of $a_\perp$. These two lengths have a simple relationship: $a_\perp/\mu = \sqrt{2\Xi}$. For example, at $\Xi = 20$, $q_0 = 2$, $T = 300$ K, and $\epsilon_d = 79$ (water), we get $a_\perp = 7.92$ Å and $\mu = 1.4$ Å.

In Fig. 1, the density ratio $\tilde{\rho}_{rel} \equiv \tilde{n}(0)/\tilde{n}(\tilde{d}/2)$ in the strong-coupling regime is plotted as a function of the above parameters for the fundamental harmonic charge modulations $[(p,q) = (1,0)$ and $(p,q) = (0,1)]$. It can be seen from Fig. 1(a) that, in the strong-coupling limit ($\Xi = 10^4$), as the plate distance d becomes greater, $\tilde{\rho}_{rel}$ becomes greater (contrary to the homogeneous surface charge distribution case which does not show variation in d). A sufficiently large coupling parameter $\Xi = 10^4$ is used for Fig. 1(a) to keep $Q_0\tilde{d}_\perp = d/a \simeq (1/\sqrt{2\Xi})d/\mu$ $(1/\sqrt{2\Xi})d/\mu$ from being large. A higher charge modulation amplitude ϵ yields greater $\tilde{\rho}_{rel}$ as expected [Fig. 1(b)]. A greater coupling parameter Ξ also yields a higher $\tilde{\rho}_{rel}$ value for the same normalized depth $D/a_\perp$ [Fig. 1(c)]. However, we need to be careful here that the coupling parameter Ξ is a function of $a_\perp$ ($a_\perp \propto \Xi^{-1/2}$). Thus, as Ξ increases, the actual charge depth D must decrease if we keep $D/a_\perp$ constant. Greater charge valence results in smaller $\tilde{\rho}_{rel}$ [Fig. 1(d)]. This originates from the fact that the counterions of higher valence tend to experience surface charges more uniformly, due to the coarse graining effect.

In Fig. 1(a), we kept the ratio d/a from being large to keep the surface charge inhomogeneity effect alive. This can be easily understood from Eqs. (5), (2), and (3). When the plate-to-plate distance d is much greater than the surface charge lattice distance a, it can be easily seen that $Q_0\tilde{d} \gg 1$ makes $\Gamma_\pm(\tilde{z}) \to 0$. This yields $I_0^2 \to 1$, leading to the uniform charge result $\tilde{n}_\pm(\tilde{z}) = 2/d$ from Eq. (5).

From the monotonic nature of the I_0^2 function in Eq. (5) and the form of $\Gamma_\pm$ in Eqs. (2) and (3), it can also be easily

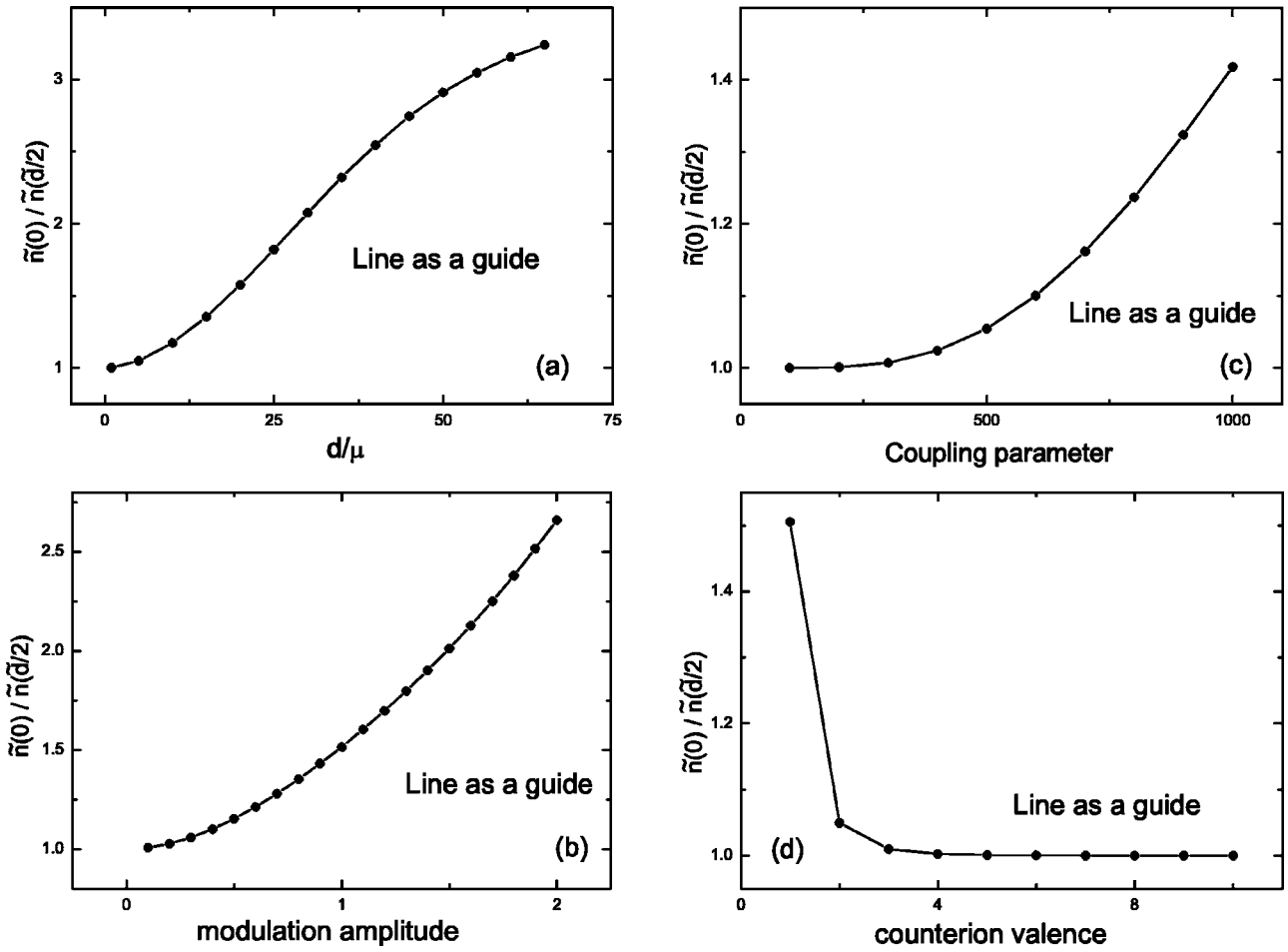

FIG. 1. (a) Counterion localization ratio as a function of plate distance $\tilde{d}$. Circular dots, data points. $\epsilon=1$, $q=2$, $\Xi=10\,000$, $D/a_\perp=0.4$ have been used. μ is the Guoy-Chapman length, $\tilde{n}_0$ is the counterion density at the plate surfaces, and $\tilde{n}(\tilde{d}/2)$ is the counterion density at the midplane between the two surfaces. (b) Counterion localization ratio as a function of surface charge modulation amplitude. Circular dots represent the numerical results. $q=2$, $\Xi=500$, $\tilde{d}=10$, and $D/a_\perp=0.3$ have been used. (c) Counterion localization ratio as a function of coupling parameter. Circular dots represent the numerical results. $\epsilon=1$, $q=2$, $\tilde{d}=10$, and $D/a_\perp=0.3$ have been used. (d) Counterion localization ratio as a function of the counterion valence. Circular dots represent the numerical results. $\epsilon=1$, $\Xi=100$, $\tilde{d}=10$, and $D/a_\perp=0.3$ have been used.

seen that the out-of-phase charge inhomogeneity tends to localize counterions at the plates more than in the in-phase case. This may be explained by the fact that the symmetry breaking of the modulated surface charge distributions between two surfaces tends to make the association of the counterions with one surface easier; i.e., the effective potential experienced by the counterions is locally asymmetric along the z direction. However, this does not necessarily mean that the attractive force between the two plates is greater for the out-of-phase surface charge inhomogeneity case, as will be shown later.

Next, we study the effect of the higher Fourier modes on the surface charge modulation (to model the effect of small charge size compared to the lattice size a). There are now numerous terms involved in the analysis, requiring a numerical treatment. As an example to show how the higher Fourier modulations affect the counterion density distribution, we use here terms from the first coupling mode $(p,q)=(1,1)$, in addition to the fundamental modes (0,1) and (1,0) discussed above. The potential up to this order is easily obtained to be

$$\tilde{u} \simeq \Gamma_\pm^0[\cos(Q_0\tilde{x})+\cos(Q_0\tilde{y})]+\Gamma_\pm^{1,1}\cos(Q_0\tilde{x})\cos(Q_0\tilde{y}),$$

and the counterion density can be expanded in $\Gamma_\pm^{1,1}$ to yield

$$\begin{aligned}\langle\tilde{n}_\pm(\tilde{x},\tilde{y},\tilde{z})\rangle_{(x,y)} &\int_0^{\tilde{d}} d\tilde{z}\, I_0^2[\Gamma_\pm(\tilde{z})]/2 \\ &= \sum_{n=0}^{\infty}(-1)^n\frac{\Gamma^n}{n!}\left(\frac{\partial^n}{\partial\Gamma_0^n}I_0[-\Gamma_\pm^0(\tilde{z})]\right)^2 \\ &= I_0^2(\Gamma_\pm^0(\tilde{z}))-\Gamma_\pm^{1,1}(\tilde{z})I_1^2[-\Gamma_\pm^0(\tilde{z})]+\frac{(\Gamma_\pm^{1,1})^2}{2}\frac{1}{2^2}(I_0+I_1)^2 \\ &+\cdots,\end{aligned}$$

where $\langle\cdots\rangle_{(x,y)}$ denotes the spatial average over x and y. Thus, unless we evaluate the integral numerically, we will be left with infinite series summations. All the higher harmonic

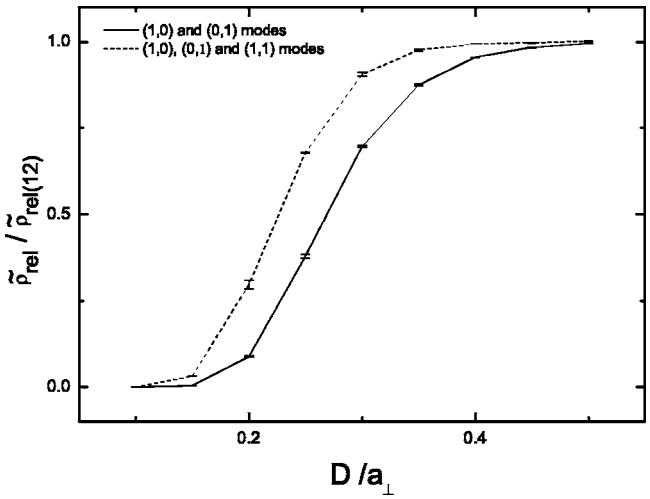

FIG. 2. Importance of the first cross component (1,1), in addition to the fundamental [(1,0) and (0,1)] Fourier modulations of the surface charge distribution at various charge depths. $q=2$, $\Xi=200$, $\tilde{d}=10$, and out-of-phase charge distribution have been used. Error bars represent integration error.

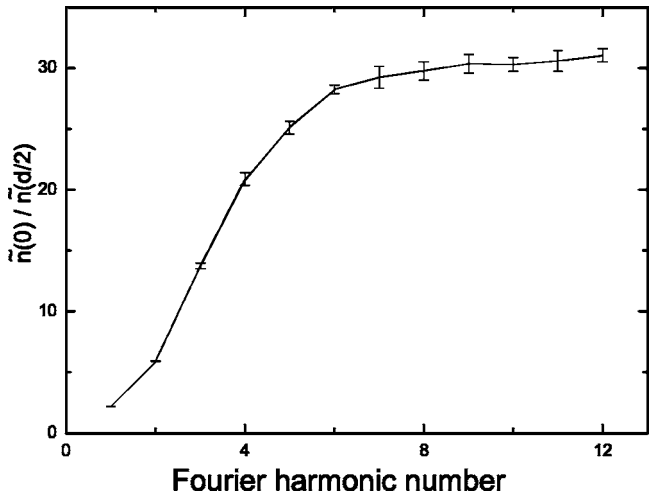

FIG. 3. Counterion localization as a function of the Fourier modulation numbers. $q=2$, $\Xi=200$, $\tilde{d}=10$, and $D/a_\perp=0.3$ have been used. The charge distributions are out of phase. Error bars represent integration error.

contributions to the counterion density and other physical quantities involve numerical integrations. In passing, it can be seen that the (1,1) harmonic contribution vanishes more quickly than the fundamental harmonic contributions for a large charge depth D due to the f_{pq} factor in Eq. (1)

$$\Gamma_{\pm}^{0} \propto \exp(-2\pi\tilde{D}),$$

$$\Gamma_{\pm}^{1,1} \propto \exp(-2\pi\sqrt{2}\tilde{D}).$$

In order to obtain validity of the lower order harmonic approximation to the surface charge modulation with respect to the charge depth D, we have evaluated the density variation ratio $\tilde{\rho}_{rel}$ from the two lowest order harmonic approximations relative to a higher harmonic modulation reference result $(p,q\leqslant 12)$ as a function of D (see Fig. 2). The adequateness of $(p,q\leqslant 12)$ to represent the discrete surface charge distribution is justified in the next section from a numerical study. The integration error bars from numerical analysis are shown together in Fig. 2. It can be seen that (A) at a shallow surface charge depth, the discrete surface charge effect is not well represented at all by either of the lower Fourier harmonic modulations; (B) at a large surface charge depth the discrete surface charge effect is well described by both of the low harmonic modulation approximations ($D/a_\perp>0.5$ for fundamental and $D/a_\perp>0.4$ for first coupling modulations). Order-by-order Fourier contributions in the counterion density localization $\tilde{\rho}_{rel}$ are plotted in Fig. 3, showing that the counterion localization effect becomes stronger as the surface charge modulation becomes closer to a discrete lattice distribution. Figure 3 also shows that the discrete particle effect reaches a reasonable saturation at harmonic number ~ 10. The level of saturation is studied against numerical simulations and found to be physically reasonable, as will be demonstrated in the next section.

At this point, we go back to the surface charge modulation at fundamental Fourier modes (0,1) and (1,0) and study their effect on the pressure in the strong-coupling limit. We note here again that the results presented here are for point counterions. Even though using the fundamental modes only may not lead us to a general conclusion for discrete surface charge effects since it is only valid for $D/a_\perp>0.5$, the basic physical properties can be more clearly identified in this system due to the minimum number of terms. This study makes it easier to understand the results from numerical simulations, to be presented in the next section. Utilizing the contact value theorem [17], the normalized pressure, which is averaged over the surface direction (x,y), is easily evaluated for fundamental Fourier modes to yield (see Appendix A)

$$\tilde{P}_{\pm}(\tilde{d}) = \left(\frac{2}{\tilde{d}}-1\right) + \frac{2}{\tilde{d}}\left(\frac{I_0^2[\Gamma_{\pm}(\tilde{d})]}{(1/\tilde{d})\int_0^{\tilde{d}} d\tilde{z} I_0^2[\Gamma_{\pm}(\tilde{z})]} - 1\right) \pm 4\epsilon_0^2 e^{-Q_0\tilde{d}} \mp \frac{8\epsilon_0}{\tilde{d}}\int_0^{\tilde{d}} d\tilde{z}\, e^{-Q_0(\tilde{d}-\tilde{z})}\frac{I_0(\Gamma_{\pm})I_1(\Gamma_{\pm})}{(1/\tilde{d})\int_0^{\tilde{d}} d\tilde{z} I_0^2(\Gamma_{\pm})}. \tag{6}$$

The various terms on the right hand side are from different physical origins. The first term $(2/\tilde{d}-1)$ is the contribution from the (0,0) Fourier mode, corresponding to uniform surface charge distribution. More specifically, this term can be broken into three pieces $(2/\tilde{d}-2+1)$ according to the physical origins, where $2/\tilde{d}$ is the entropic pressure among the counterions, -2 is the attractive electric interaction between the counterions and the surface ions, and $+1$ is the repulsive electric interaction between two surface charges. This term $(2/\tilde{d}-1)$ can be positive (repulsive) or negative (attractive) depending upon the plate-to-plate distance $\tilde{d}$. This behavior

between two homogeneously charged plates has already appeared in the literature [9,10]. All the other terms represent modifications to this term from the surface charge inhomogeneity effects.

The second term is the increase in the entropic pressure in the counterions from the (1,0) and (0,1) inhomogeneity of the surface charge distribution. It is always positive due to the localization of the counterions toward the plate surface by the surface charge inhomogeneity. This term decays faster than $1/\tilde{d}$ as $\tilde{d}$ becomes small since the surface charge modulation effect on counterion distribution small.

The third term represents modification in the electric interaction between two charged surfaces due to their (1,0) and (0,1) Fourier components. This term is positive if the relative surface charge distribution is in phase because equally modulated charges are facing each other, and negative if out of phase because oppositely modulated charges are facing each other. The effect of this term can easily be found intuitively.

The fourth term is the modification to the surface-to-counterion electric interaction by the surface charge inhomogeneity. Counterions have a tendency to be aligned with the nearer surface charge modulation. Since the interacting charges here have opposite signs, unlike in the third term, the fourth term is negative if the surface charge distribution is in phase because all the counterions tend to be aligned in phase with the surface anion modulations [reducing the average distance and potential energy between the surface charges and counterions averaged over the thermal motions; see Fig. 4(a)]. On the other hand, if the two surface charges are out of phase, roughly half of the counterions are out of phase with the surface ions [see Fig. 4(b)]. It turns out that this misalignment between the surface anions and the counterions can enhance the average anion-cation distance averaged over the thermal motions and, thus, raise the pressure above that in the in-phase case. This term can oppose the phase effects from the third term, and may be greater than the third term in the strong-coupling regime. We find from our numerical studies that the behavior of this term is a complicated function of counterion valence, temperature, plate-plate distance, and other physical parameters. For example, monovalent counterions are more closely localized to the plate surfaces and, thus, half of the counterion interactions with the other surface are reduced unless the plate-to-plate distance becomes near or smaller than the Gouy-Chapman distance (in which case the finite thermal motion spreads the counterions evenly in z between the two plates). Thus, the fourth term may not be as strong as that in the divalent counterion case unless the plate-to-plate distance becomes smaller than the Gouy-Chapman distance. If the counterion temperature approaches 0 K, then the higher pressure tendency for monovalent counterions remains valid even at plate distances near or smaller than the Gouy-Chapman distance. If the plate-to-plate distance is reduced much below the Gouy-Chapman length, the counterion alignment with the surface ions is destroyed due to the strong repulsive force between the counterions in the z direction. This causes a global misalignment of the counterions and can raise average distance between the surface charges and counterions, sharply increasing the pressure. The discussions presented here are also dependent upon the surface charge depth, which reduces the charge inhomogeneity effect. Actual examples will be presented in the next section.

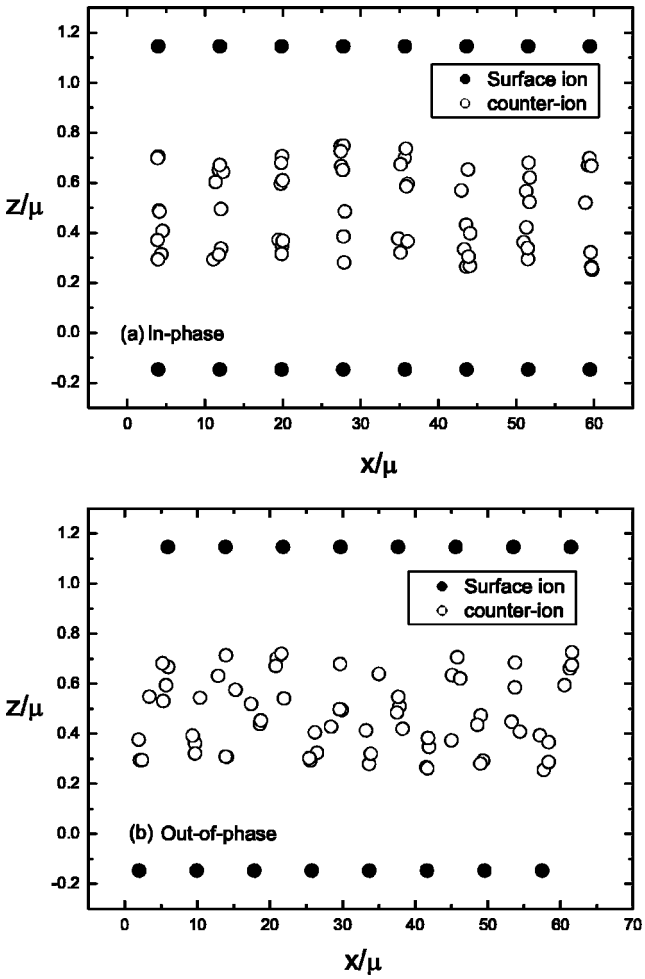

FIG. 4. Spatial configuration of counterion and surface charges for (a) in-phase and (b) out-of-phase surface charge configurations, showing better lateral alignment of the counterions with the surface charges for the in-phase configuration.

In Eq. (6), where the surface charge modulation is described by the fundamental Fourier modes only, we find that the fourth term is usually greater than the third term and the physical phenomenon in the fourth term influences the behavior of the pressure more than the third term does. Thus, the in-phase surface charges yield lower pressure than the out-of-phase charges (see Fig. 5). However, at higher values of the surface-charge inhomogeneity amplitude $\epsilon > 2$ (in this case, the surface charges are no longer pure anions), the second term becomes stronger and the out-of-phase charge distribution now yields lower pressure. Since this behavior is observed from Eq. (6), the validity of this discussion has to be confined to the case of deep embedding and fundamental modulation of the surface charge for now. From a more complete numerical simulation in the next section, we find that the in- or out-of-phase influence on the pressure depends upon the charge valence and temperature of the counterions.

Figure 6 shows the density ratio versus the normalized charge depth. As easily noticed from the figure, discrete

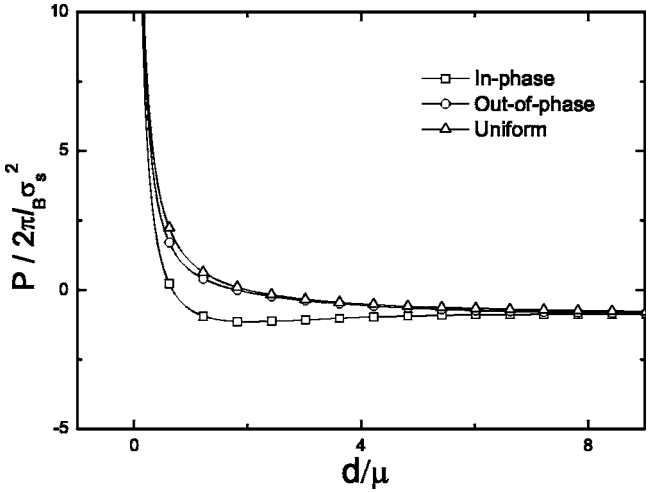

FIG. 5. Pressure as a function of plate distance for in-phase and out-of-phase charge modulation of the fundamental Fourier component. The uniform charge distribution case is shown also. $\tilde{d}=2$, $\Xi=20$, and $D/a_{\perp}=0.1$ are used.

pointlike charges embedded near the plate surface tend to strongly attract and localize the point counterions. As the charge embedding becomes deeper the discreteness effect gets weaker, and the spatial correlation between the counterions and the surface charges becomes looser. As a result the z variation in the counterion density is reduced. At $D/a_{\perp}=0.5$ the inhomogeneity effect is already significantly reduced. When the charge depth becomes much deeper, the system exhibits behavior similar to that of a uniformly charged system characterized by $\tilde{\rho}_{rel}\rightarrow 1$, as discussed earlier. It is demonstrated here again that the depth of the surface charges below the surfaces is an essential parameter and plays an important role in determining the characteristics of a discretely distributed charge system [13].

III. NUMERICAL SIMULATIONS

Two types of molecular dynamics [18] simulations are performed in the present work. In addition, a Monte Carlo simulation is used to compare with, and validate, the molecular dynamics simulations. The Lekner-Sperb and Metropolis methods are used for the Monte-Carlo [19] simulation; and two of the well-known particle simulation methods, the two dimensionally periodic particle method (MMM2D) [16,20] and the particle-particle-particle-mesh Ewald (P3ME) method [21–23], are used for the molecular dynamics simulations. The molecular dynamics codes are parallelized [24,25] and run on a local Pentium-IV cluster.

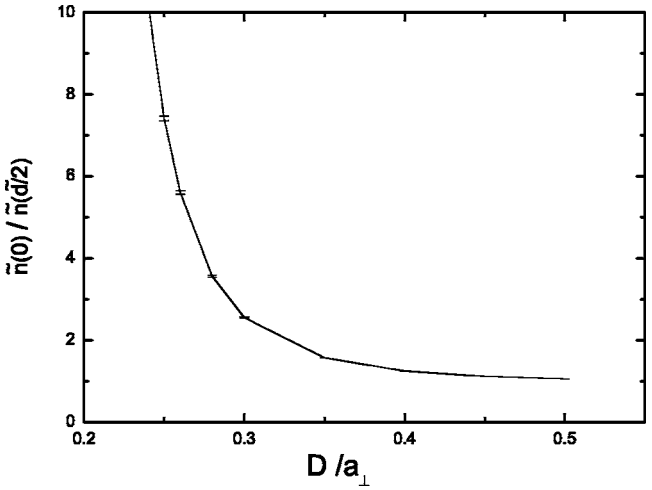

FIG. 6. Counterion localization as a function of surface charge depth $D/a_{\perp}$. $q=2$, $\Xi=200$, and $\tilde{d}=10$ are used.

The MMM2D particle simulation method is adequate for systems that are periodic in two dimensions (2D) and finite in the other direction (2D+h system), and guarantees a highly accurate field calculation. Its drawback, however, is the large amount of computational time needed. The P3ME method is based on a combined use of particle and mesh techniques to reduce the cost in computational time. Although P3ME was originally developed for three-dimensional systems [16,26–30], an adaptive scheme based on the dipole corrections [29] and layer correction method [16] is applicable to the situation (2D+h) considered here. The molecular dynamics results shown in the present work have been cross verified by the MMM2D and P3ME methods. The simulation methods used in the present work are not new. For the sake of completeness, we briefly describe the methods in Appendix B. For a more complete description of the numerical methods, we refer interested readers to the above listed references.

Simulations are performed using a regular two-dimensional latticelike distribution of point surface charges at a depth D. Pointlike counterions are assumed to be in thermal contact with a thermal reservoir at a normalized temperature (300 K and the dielectric constant of water are used unless otherwise stated). With pointlike discrete surface charges, it has been observed from the simulation that if the initial counterion distribution is asymmetric in z, the counterion density distribution remains asymmetric over a long simulation time. This asymmetric state may be regarded as a metastable state because in a true equilibrium state, the counterions should be distributed symmetrically. The reason for this long-surviving metastable state might be the strong coupling between counterions and surface charges (i.e., the strong counterion attraction to the surface charges slow down the symmetrizing process). The dynamics of the metastable physics should be studied more carefully; in this paper only the final equilibrium physics is considered. To achieve the symmetric state quickly, the initial counterion configuration is chosen artificially such that the number of counterions is the same at both sides of the midplane between the two plates.

Due to the approximation methods used in the analytic progress, we find that it is necessary to verify the strong and inhomogeneous interaction physics by a numerical simulation. Several important physics features appear in the numerical studies which were not evident in the analytic studies. In Fig. 7 a typical simulation result is compared with analytic results, varying the order of the Fourier modulation in the analytic results. The plate distance $d=2\mu$ has been chosen since that is approximately where the minimum pressure appears often. The coupling parameter $\Xi=20$ is used. As the order of Fourier modulation is increased, the analytic

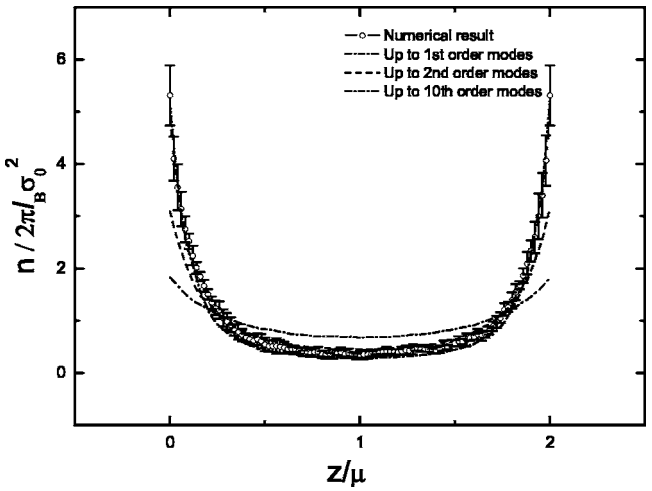

FIG. 7. Numerical counterion density profile between two plates for a discrete surface charge distribution. Charges are strongly localized to the plate surface. The analytic curves with a few charge modulation cases are shown together for comparison. $\Xi=20$ and $D/a_\perp=0.1$ are used.

counterion density profile approaches the numerical result obtained from a discrete surface charge distribution. When we include up to the tenth Fourier modes or higher, the analytic result approaches the numerical result within the error bar of the numerical result, with a strong localization of counterion density toward the plate surfaces. This verifies the observation made in the previous analytic section that the discrete surface charge effect can be reasonably modeled with Fourier modulation number of about 10. Another observation to be noted here is the appearance of the strong-coupling effect at a lower coupling parameter. In a uniform surface charge distribution the strong-coupling effect arises at a much higher coupling parameter $\Xi>100$, as observed in Ref. [1]. But in a discrete surface charge distribution, the strong-coupling effect appears at a lower coupling parameter $\Xi=20$ as confirmed in Fig. 7. This also verifies the validity of the strong-coupling theory at Ξ as low as 20, as mentioned in the previous section. The lower Ξ boundary for the strong-coupling phenomenon is a function of many physical parameters. A systematic study of the lower Ξ boundary is left as a future research topic.

The pressure (normalized to $2\pi l_B\sigma_s^2$) between two plates is plotted in Fig. 8 for a discrete surface charge distribution for (a) $D/a_\perp=0.1$ and (b) $D/a_\perp=0.05$. As usual, divalent counterions are used. Figure 8(a) is to be compared to the simplest analytic result shown in Fig. 6, which is obtained from a modulated surface charge distribution with fundamental Fourier harmonic modes only (and thus inaccurate). It can be noticed here again that the out-of-phase surface charge distribution yields higher pressure, which indicates that the surface-to-counterion interaction is stronger than the surface-to-surface interaction [see the discussion after Eq. (6) in the previous section]. It can also be noticed that the pressure minimum exists for both in- and out-of-phase surface charges. Figure 8(b) shows the sensitivity of the pressure to the surface charge depth. As the charge depth becomes shallower, the pressure exhibits a sharp minimum at $d<0.5\mu$. At

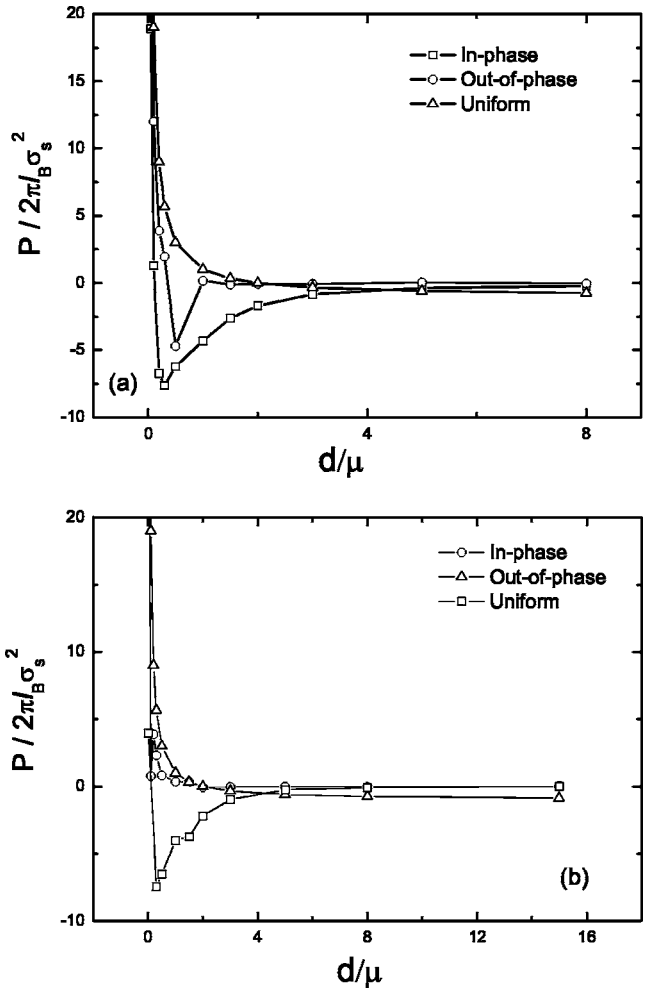

FIG. 8. Pressure versus plate distance for in-phase and out-of-phase discrete surface charge distributions with divalent counterion obtained from numerical simulation. The uniform surface charge case (analytic) is plotted also. $\Xi=20$ and $D/a_\perp=0.1$ are used in (a), while $\Xi=20$ and $D/a_\perp=0.05$ are used in (b).

such a small distance, the finite counterion size effect will come in and raise the pressure. The sharp valley shown here is for an academic purpose. The valley actually gets deeper with a higher resolution. At large plate distances ($d/a_\perp\gg1$), the pressure becomes similar to that in the uniform charge case (the normalized pressure actually approaches -1).

Figure 9 shows numerical simulation results with monovalent counterions, instead of the divalent counterions as in Fig. 8. All the other parameters are the same. It can be seen that, unlike in Fig. 8, the out-of-phase surface charge distribution yields lower pressure than the in-phase distribution here. This is due to the weakening of the surface to far-counterion interaction from higher counterion localization toward the surfaces for monovalent counterions. Thus, the surface-to-surface interaction property is now showing up, as discussed after Eq. (6). It can also be seen that the pressure for the in-phase case eventually falls sharply below the out-of-phase case at $d<0.5\mu$. This is the counterion uniformization effect in the z direction by finite thermal motions at a small plate-to-plate distance, again, as discussed after Eq. (6). The surface-to-counterion interaction is now strong

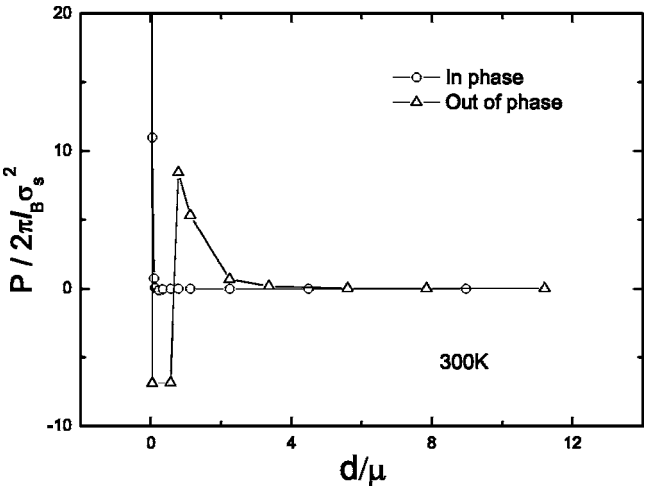

FIG. 9. Pressure versus plate distance obtained from numerical simulation for in-phase and out-of-phase discrete surface charge distributions with monovalent counterion. The uniform surface charge case (analytic) is plotted also. $\Xi=20$ and $D/a_{\perp}=0.05$ are used.

again. This effect disappears as the counterion depth approaches 0 (see Fig. 10).

IV. DISCUSSION AND CONCLUSION

In the present work, the effect of surface charge inhomogeneity on the pointlike counterion density profile and pressure between two charged plates is studied in the strong-coupling limit, using both theoretical and numerical methods. Strong-coupling theory has been analytically applied to modulated surface charges. It is shown, by comparison with numerical results, that the strong-coupling theory is applicable to a much lower coupling parameter than what is known for a uniform surface charge system when the surface charge distribution is inhomogeneous. It is found that counterions are more strongly localized to the plate surfaces as the surface charge inhomogeneity or discreteness increases. This creates a lower pressure between the two plates than that from uniform surface charges. For divalent counterions, the pressure is lower when the surface charge distributions on the two plates are in phase. However, for monovalent counterions, the pressure becomes higher with in-phase surface charge distributions at $d>\mu/2$, and then falls sharply below the out-of-phase level for $d<\mu/2$. The sharp fall behavior occurs at finite temperature at small d and disappears as the counterion depth approaches 0.

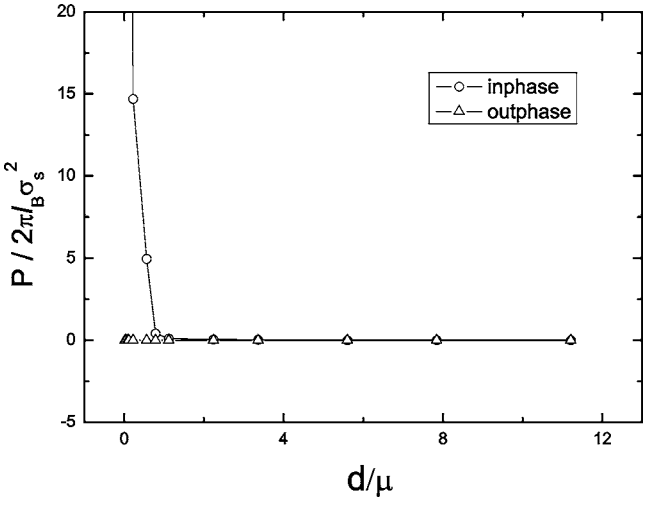

FIG. 10. Pressure versus plate distance at counterion temperature 0.3 K. Monovalent counterions are used. Numerical Monte Carlo simulation is used with the surface charge depth of $D=0.001a_{\perp}$.

The key physical parameters characterizing the interaction between two surfaces with discrete surface charges are the distance between surfaces, surface charge density, depth of surface charges beneath the surfaces, counterion valence, coupling parameter of the system, and phase relation between two surface charge configurations. At a large distance between two plates, low surface charge density, large charge depth, large valence of the counterions, or small coupling parameter, the surface charge inhomogeneity effect weakens and disappears.

We note here that as the distance between the two surfaces increases, the system cannot be explained on the basis of the strong-coupling theory alone. In this regime, counterions obey the strong-coupling theory near the plate surfaces, but are subject to the Debye-Hückel theory at a greater distance from the plates. As the distance from the surfaces increases, it is expected that the Poisson-Boltzmann theory will eventually become valid.

We also note here that the finite counterion size effect may play a role when the surface-to-surface distance becomes comparable to the counterion size. A numerical study of this effect is under progress, but requires a much more demanding computational work, and is left for a future publication.

ACKNOWLEDGMENTS

During this work, Y.S.J. and M.W.K. have been supported by Korean KISTEP under Grant No. I-03-064 and a grant of the Korea Health 21 R&D Project. G.P. and C.S.C. have been supported by the Korean Basic Science Institute. P.P. and M.W.K. have been supported by the U.S. MRSEC programs of the NSF under Grants No. DMR00-80034 and No. DMR02-037555.

APPENDIX A: DERIVATION OF EQ. (6)

In the contact value theorem, the pressure between two plates can be decomposed into two parts [32–34],

$$\frac{P}{k_BT}=n(d)-\frac{1}{k_BTL^2}\int d\vec{\rho}\,\sigma_2(\vec{\rho})E(\vec{r})|_{z=(d+D)} \qquad \text{(A1)}$$

where the first term (density) is the entropic pressure and the second term is the electric pressures at $z=d+D$, and E is the electric field. The density is given in Eq. (5),

$$\frac{n(d)}{2\pi l_B \sigma_0^2} = \frac{2I_0^2[\Gamma_\pm(d)]}{\int_0^d dz\, I_0^2[\Gamma_\pm(z)]}. \tag{A2}$$

The electric pressure is a superposition of two different interactions $P^E = P_{ss} + P_{sc}$, where P_{ss} is the pressure from surface-to-surface interaction and P_{sc} is the pressure from the surface-to-counterion interaction. The pressure from the surface-to-surface charge interaction is described by

$$P_{ss} = \frac{-l_B}{a^2}\frac{\partial}{\partial d}\sum_{\vec{m}} \int_{unit\ cell} d\vec{\rho} \int_{unit\ cell} d\vec{\rho}'\ \sigma_1(\vec{\rho})\sigma_2(\vec{\rho}') \times \frac{1}{\sqrt{(\vec{\rho}-\vec{\rho}'+a\vec{m})^2+(d+2D)^2}},$$

where $\vec{\rho}$ is the two-dimensional position vector on the (x,y) plane within a unit cell, $\sigma_1(\vec{\rho})$ and $\sigma_2(\vec{\rho})$ are the two-dimensional charge density distributions on each plate, and $\vec{m}=(m_x,m_y)$.

Applying the Poisson formula

$$\sum_{k\in\mathbf{Z}} f(x+\delta k) = \frac{1}{|\delta|}\sum_{p\in\mathbf{Z}} \mathcal{F}(f)(p/\delta)e^{(2\pi i/\delta)px} \tag{A3}$$

to $1/\sqrt{(\vec{\rho}+a\vec{m})^2+(d+2D)^2}$, where $\mathcal{F}(f)(p/\delta)$ denotes the Fourier transform of function f, we obtain

$$\begin{aligned} P_{ss} &= -2\pi l_B \frac{\partial}{\partial d}\sum_{\vec{Q}} \frac{e^{-Q(d+2D)}}{Q}\left(\frac{1}{a^2}\int_{unit\ cell} d\vec{\rho}\ \sigma_1(\vec{\rho})e^{i\vec{Q}\cdot\vec{\rho}}\right) \times \left(\frac{1}{a^2}\int_{unit\ cell} d\vec{\rho}'\ \sigma_2(\vec{\rho}')e^{-i\vec{Q}\cdot\vec{\rho}'}\right) \\ &= 2\pi l_B \sum_{\vec{Q}} e^{-Q(d+2D)}\sigma_1(\vec{Q})\sigma_2(-\vec{Q}) \\ &= 2\pi l_B \sigma_0^2 + 2\pi l_B \sum_{\vec{Q}\neq 0} e^{-Q(d+2D)}\sigma_1(\vec{Q})\sigma_2(-\vec{Q}) \end{aligned} \tag{A4}$$

where $Q=|\vec{Q}|$ and $\vec{Q}=(2\pi/a)(p_x,p_y)$ with p_x,p_y being integer numbers. Considering only the fundamental Fourier mode for σ_1 and σ_2, we then obtain

$$P_{ss} = 2\pi l_B \sigma_0^2 (1 \pm 4\epsilon_0^2 e^{-Q_0(d+2D)}). \tag{A5}$$

The first term is the contribution from the (0,0) mode of the surface charge and the second term is the modified contribution from the fundamental Fourier modes $(0,\pm 1),(\pm 1,0)$.

The surface-to-counterion contribution P_{sc} can be written in the form

$$P_{sc} = \frac{q_0 l_B}{L^2}\int_0^d dz \int d\vec{\rho}\, n_\pm(\vec{\rho},z)\frac{\partial}{\partial d} \times \left(\sum_{\vec{m}} \int_{unit\ cell} d\vec{\rho}' \frac{1}{\sqrt{(\vec{\rho}-\vec{\rho}'+a\vec{m})^2+(z-d-D)^2}}\sigma_2(\vec{\rho}')\right)$$

where q_0 is the counterion valence and $n_\pm$ is given in Eq. (5). This integral can be evaluated in a similar manner as for P_{ss} to yield, for the fundamental surface charge modulation only,

$$P_{sc} = -4\pi l_B \sigma_0^2 \mp 16\pi l_B \sigma_0^2 \epsilon_0 \times \int_0^d dz\, e^{-Q_0(d+2D-z)} \frac{I_0(\Gamma_\pm)I_1(\Gamma_\pm)}{\int_0^d dz\, I_0^2[\Gamma_\pm(z)]}. \tag{A6}$$

Again, the first term represents the (0,0) mode, and second term represents the fundamental mode contribution.

Adding up Eqs. (A2), (A5), and (A6) and normalizing each term, we obtain

$$\begin{aligned} \tilde{P}_\pm(\tilde{d}) &= \left(\frac{2}{\tilde{d}} - 1\right) + \frac{2}{\tilde{d}}\left(\frac{I_0^2[\Gamma_\pm(\tilde{d})]}{(1/\tilde{d})\int_0^{\tilde{d}} d\tilde{z}\, I_0^2[\Gamma_\pm(\tilde{z})]} - 1\right) \\ &\quad \pm 4\epsilon_0^2 e^{-Q_0(\tilde{d}+2\tilde{D})} \mp \frac{8\epsilon_0}{\tilde{d}}\int_0^{\tilde{d}} d\tilde{z}\, e^{-Q_0(\tilde{d}+2\tilde{D}-\tilde{z})} \times \frac{I_0(\Gamma_\pm)I_1(\Gamma_\pm)}{(1/\tilde{d})\int_0^{\tilde{d}} d\tilde{z}\, I_0^2(\Gamma_\pm)}, \end{aligned}$$

which is Eq. (6).

APPENDIX B: SIMULATION METHODS

In the Monte Carlo simulation of the counterions, the Lekner-Sperb [2] and Metropolis [19] schemes are used for the evolution of the particle system to minimize the free energy by random sampling of the particle configurations. The transition probability to go from an old configuration to a new trial configuration is governed by the detailed balance condition [19] in a canonical ensemble,

$$\frac{\mathcal{P}(o\to n)}{\mathcal{P}(n\to o)} = \exp\{-\beta[\mathcal{U}(n)-\mathcal{U}(o)]\}$$

where o denotes the old configuration of the system, n denotes the new trial configuration, β denotes the Boltzmann factor, and $\mathcal{U}(i)$ is the potential energy of the system. Then, the accepted probability of a trial move becomes

$$\mathcal{P}(o\to n) = \min(1,\exp\{-\beta[\mathcal{U}(n)-\mathcal{U}(o)]\}).$$

New particle positions are randomly sampled and acceptance according to the acceptance probability $\mathcal{P}$.

Molecular dynamics methods (MMM2D and P3ME) solve the particle trajectories of the model system by solving an equation of motion. Since the systems of interest are within the canonical ensemble, instead of solving the deterministic Newton's equation, we solve the Langevin equation,

$$m_i \ddot{r}_i = -\nabla U(r_i) - \Gamma \dot{r}_i + \xi_i(t)$$

where $\langle \xi_i(t)\rangle = 0$ and $\langle \xi_i(t)\xi_j(t')\rangle = 6k_B T\Gamma\delta_{ij}\delta(t-t')$, m_i is the mass of particle i, and Γ is the friction coefficient. Most of the simulation time is spent in calculating the interaction potential and force.

The system considered here consists of an infinite number of periodic cells in two dimensions and a finite size in the

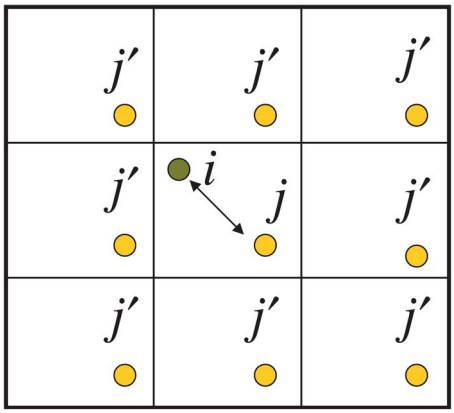

FIG. 11. (Color online) Interaction of the jth particle with the j'th particle within the cell is extended to all the periodic image charges in the infinite number of periodic cells.

other direction (2D+h geometry). The Lekner-Sperb and MMM2D methods directly sum the potential and force with all periodic images after converting them to a rapidly convergent formula, as depicted in Fig. 11,

$$E = \sum_{i \neq j} \sum_{\vec{n}} \frac{q_i q_j}{|\vec{r}_i - \vec{r}_j + \vec{n}|}$$

where $\vec{n}$ denotes a reciprocal vector. The computational effort of this direct method is basically $O(N^2)$. MMM2D separates potentials into a near formula and a far formula in a finite direction. If only the near formula is accounted for, MMM2D gives the same result as the Lekner-Sperb formula. Applying factorization on the far formula, MMM2D can be accelerated to an $O(N^{5/3})$ scaling.

The P3M method is based on the combined use of the particle and mesh methods to reduce the cost in computational time [16,26–30]. P3ME applies P3M to the Ewald method [21,22]. The Ewald method splits the potential into two parts:

$$\frac{1}{r} = \frac{\mathrm{erfc}(r)}{r} + \frac{1 - \mathrm{erfc}(r)}{r}$$

where $\mathrm{erfc}(r) = (2/\sqrt{\pi}) \int_r^\infty dt\, e^{-t^2}$. Then, the Ewald formula for the electrostatic potential is

$$E = E^{(r)} + E^{(k)} + E^{(s)} + E^{(d)},$$

$$E^{(r)} = \frac{1}{2} \sum_{i \neq j} \sum_{\vec{n}} q_i q_j \frac{\mathrm{erfc}(\alpha |\vec{r}_i - \vec{r}_j + \vec{n}|)}{|\vec{r}_i - \vec{r}_j + \vec{n}|},$$

$$E^{(k)} = \frac{1}{2} \sum_{\vec{n}} \sum_{k \neq 0} \frac{4\pi}{k^2} e^{-k^2/4\alpha^2} |\rho(k)|^2,$$

$$E^{(s)} = -\frac{\alpha}{\sqrt{\pi}} \sum_i q_i^2,$$

$$E^{(d)} = \frac{2\pi}{\sqrt{3}V} \left(\sum_i q_i r_i \right)^2. \tag{B1}$$

The first term is from the interactions in real space, the second term is from the reciprocal space [$\rho(k)$ is the Fourier transformed density], the third term is the self-energy, and the fourth term is from the dipole correction. α is the Ewald parameter, which assigns the portions of the real space contribution and reciprocal contribution. The result is expected to be independent of α. The first term decays fast over the cutoff distance. The second term is a slowly varying function over the entire distance. Thus, the Fourier components can be expressed by only the few lowest components. Applying these Fourier components to the P3M method, the computational cost is reduced to $O(N \log N)$. Although P3M was originally developed for a three-dimensional system, the adaptive scheme based on the dipole corrections [29] in Eq. (B1) and the layer correction method [16] are applicable to the (2D+h) system considered here [31].

[1] R. R. Netz, Eur. Phys. J. E **5**, 557 (2001).
[2] A. G. Moreira and R. R. Netz, Eur. Phys. J. E **8**, 33 (2002).
[3] A. W. C. Lau and P. Pincus, Phys. Rev. E **66**, 041501 (2002).
[4] B. I. Shklovskii, Phys. Rev. E **60**, 5802 (1999).
[5] Hiroshi Frusawa, J. Phys. Soc. Jpn. **73**, 507 (2004).
[6] Z. Donko and G. J. Kalman, Phys. Rev. E **63**, 061504 (2001).
[7] S. A. Safran, *Statistical Thermodynamics of Surfaces, Interfaces, and Membranes* (Addison-Wesley, Reading, MA, 1994).
[8] I. Rouzina and V. A. Bloomfield, J. Phys. Chem. **100**, 9977 (1996).
[9] L. Guldbrand, B. Jönson, H. Wennerström, and P. Linse, J. Chem. Phys. **80**, 2221 (1984).
[10] B. Y. Ha, Phys. Rev. E **64**, 031507 (2001).
[11] R. R. Netz, Phys. Rev. E **60**, 3174 (1999).
[12] A. G. Moreira and R. R. Netz, Europhys. Lett. **52**, 705 (2000).
[13] A. G. Moreira and R. R. Netz, Europhys. Lett. **57**, 911 (2002).
[14] D. B. Lukatsky and S. A. Safran, Europhys. Lett. **60**, 629 (2002).
[15] M. L. Henle, C. D. Santangelo, D. M. Patel, and P. A. Pincus, Europhys. Lett. **66**, 284 (2004).
[16] A. Arnold and C. Holm, Comput. Phys. Commun. **148**, 327 (2002).
[17] D. Henderson and L. Blum, J. Chem. Phys. **69**, 5441 (1978).
[18] J. Qiang and S. Habib, Phys. Rev. E **62**, 7430 (2000).
[19] D. Frenkel and B. Smit, *Understanding Molecular Simulation* (Academic Press, San Diego, 1996).
[20] A. Arnold, J. Joaniss, and C. Holm, J. Chem. Phys. **117**, 2496 (2002).
[21] M. Deserno and C. Holm, J. Chem. Phys. **109**, 7678 (1998).
[22] M. Deserno and C. Holm, J. Chem. Phys. **109**, 7694 (1998).
[23] R. W. Hockney and W. Eastwood, *Computer Simulation Using Particles* (IOP, Bristol, 1998).

[24] Y. Aoyama and J. Nakano, *RS/6000SP:Practical MPI Programming* (IBM Redbooks, Tokyo, Japan, 1999).
[25] S. Plimpton and B. Hendrickson, J. Comput. Chem. **17**, 326 (1996).
[26] R. R. Netz, J. Phys.: Condens. Matter **16**, S2353 (2004).
[27] E. R. Smith, Proc. R. Soc. London, Ser. A **375**, 475 (1981).
[28] B. A. Luty, I. G. Tironi, and W. F. Gunsteren, J. Chem. Phys. **103**, 3014 (1995).
[29] I. C. Yeh and M. L. Berkowitz, J. Chem. Phys. **111**, 3155 (1999).
[30] E. L. Pollock and J. Glosli, Comput. Phys. Commun. **95**, 93 (1996).
[31] M. Kawata and M. Mikami, J. Chem. Phys. **116**, 3430 (2002).
[32] D. Henderson and L. Blum, J. Chem. Phys. **69**, 5441 (1978).
[33] S. L. Carnie and D. Y. C. Chan, J. Chem. Phys. **74**, 1293 (1981).
[34] R. R. Netz and H. Orland, Eur. Phys. J. E **1**, 203 (2000).